DOI 10.2478/ama-2024-0005

FATIGUE BEHAVIOUR OF MEDIUM CARBON STEEL ASSESSED BY THE BARKHAUSEN NOISE METHOD

Katarzyna MAKOWSKA*, Tadeusz SZYMCZAK **, Zbigniew L. KOWALEWSKI ***

*Faculty of Mechatronics, Armament and Aerospace, Military University of Technology,
ul. gen. Sylwester Kaliski 2, 00-908 Warsaw, Poland
**Department of Vehicle Type-Approval & Testing, Motor Transport Institute, ul. Jagiellonska 80, 03-301 Warsaw, Poland
***Department of Experimental Mechanics, Institute of Fundamental Technological Research of the Polish Academy of Sciences,
ul. Pawinskiego 5B, 02-106 Warsaw, Poland

katarzyna.makowska@wat.edu.pl, tadeusz.szymczak@its.waw.pl, zkowalew@ippt.pan.pl

received 26 April 2023, revised 30 June 2023, accepted 6 July 2023

Abstract: In this paper, an attempt to estimate the stage of the fatigue process using the Barkhausen noise method is studied. First, microstructural and static tensile tests were carried out and, subsequently, fatigue tests up to failure were conducted. After determination of the material behaviour in the assumed static and dynamic conditions, the interrupted fatigue tests were performed. Each specimen was stressed up to a different number of cycles corresponding to 10%, 30%, 50%, 70% and 90% of fatigue lifetime for the loading conditions considered. In the next step of the experimental programme, the specimens were subjected to the Barkhausen magnetic noise measurements. Various magnetic parameters coming from the rms Barkhausen noise envelopes were determined. The linear relationship betweenthe full-width at half-maximum (FWHM) of the Barkhausen noise envelope and the number of loading cycles to fracture was found. Specimens loaded up to a certain number of cycles were also subjected to a tensile test to assess an influence of fatigue on the fracture features.

Keywords: fatigue, Barkhausen noise, structural steel, fracture, mechanical properties, deformation

1. INTRODUCTION

It is well known that failures of 90% of working parts occur due to fatigue [1, 2]. The following components can be indicated as typical examples of such cases: crankshaft [4, 3], driveshaft [5], shaft [6] and idler gear [7]. They are usually investigated by means of different experimental techniques such as macrophotography [3, 6] or scanning electron microscopy (SEM) [4, 5]. These methods enable to identify quite easily a crack focus, fatigue lines and fringes, damage zone and crack orientation, and permanent deformation in micro-regions. It has to be emphasised however, that they represent destructive techniques, which involve specimen selections at the operational stage or after a specific technical incident. As a result, they lead to the solution of the inverse task, providing information about possible reasons for the crack or component separation only. From a practical point of view, an important issue is the influence of evaluation of fatigue cycles on material properties and technical condition assessment of the element without any physical interference in its geometry and properties. Therefore, non-destructive methods such as ultrasonic [8, 9], magnetic-particle [10] and Barkhausen noise [11, 12] can be relatively very helpful.

The ultrasonic method is the technique most often used in many branches of contemporary industry: automotive [13, 14], aviation [15-17], power engineering and building [18, 19]. However, it should be noted that conventional ultrasonic parameters such as the wave velocity and attenuation coefficient have some limits in applications. The non-homogeneity of the microstructure, construction geometry and thickness assessment of the elements tested are the main difficulties in the wave velocity measurements. In the case of attenuation coefficient, a difficulty appears in elimination of the influence of material non-homogeneity and surface geometry [20]. In literature [21] the results at zero-to tension cycles on polycrystalline 99.99 mass % copper are discussed. Attenuation coefficient α, and plate thickness resonant frequencies fn, were measured using electromagnetic acoustic resonance (EMAR) [21].

The attenuation coefficient α is known as follows:

$$\alpha = \left(\frac{16GBb^2}{\pi^4 C^2}\right) \wedge L^4 f^2, \text{ represents} \tag{1}$$

where G is the shear modulus, Λ is the dislocation density, B is the damping constant, L is the dislocation loop length, b is the Burgers vector magnitude, C is the dislocation-line tension and f is the ultrasonic excitation frequency. The plate thickness resonant frequency can be calculated using the following expression:

$$f_n = nV \,/\, (2d), \tag{2}$$

where n is the integer identifying the mode, V is the shear wave velocity and d is the thickness of the plate.

Simultaneously, transmission electron microscopy (TEM) was used to follow the evolution of dislocation microstructure at the fatigue life. Three levels of stress: 105 MPa, 110 MPa and 115 MPa were used and the following values of the cycle number to fracture were obtained, respectively: N_f = 253 800, N_f = 116 000 and N_f = 41 250.

The feature of ultrasonic parameter changes can be divided into four stages. In the first stage attenuation coefficient α is constant and plate thickness values of frequency f_n slowly increase. Two processes occur in the material. There is an ongoing process of multiplication dislocation, which leads to an increase Λ, and the process of tangling causes a decrease in L. This keeps the dislocation damping nearly stable [21].

In the second stage, the coefficient α increases markedly. Also, the value of f_n increases. Dislocation multiplication and movement beneath the specimen's surface occur through dislocation slips within the period representing 10% of the specimen fatigue life. The dislocation network is completely reorganised. Dislocations are released from heavy tangling and microstructural features and create stable cell structures [21]. According to Eq. (1) [21], dislocation loop length L increases, which leads to a significant increase in α values due to the power relation $\alpha \sim L^4$. A slight drop in α observed just before the maximum can be attributed to the reduced dislocation mobility caused by the heavy tangling and pilling-up just before dislocation reorganisation [21].

In the third stage of the loading process, values of the α coefficient α decrease; however, its values are not lower than those obtained in the first stage of fatigue. Contrary to that, the f_n increases as the slip bands decrease. The dislocation mobility is suppressed because of the deceleration of increased slip-band density. As a consequence, dislocations become stationary even to the order of 0.1 nm or less values of ultrasonic amplitude [21]. Dislocations of cell structure have less mobility, and therefore, they are responsible for fatigue hardening [21].

Coefficient α decreases slightly in the last stage, while f_n increases since the formation of cell walls is completed and only a very few free dislocations occur in the material considered [21].

Luo et al. [22] analysed an early stage of the pure iron damage due to fatigue carried out for R = -1, f = 0.1 Hz and constant stress amplitude equal to 160 MPa. A triangle waveform was applied. The fatigue was interrupted after 1, 2, 5, 10, 25, 100 and 1000 cycles. Each loading process was performed on the individual specimens separately. Two ultrasonic methods were applied. The first one was based on the measurements of longitudinal wave L_{CR} amplitude reflected at the first critical angle, then propagating beneath and parallelly to the surface [22]. The pulse-echo mode was the second ultrasonic method applied.

According to the first testing method, a new damage parameter was proposed in the following form:

$$A_{dif} = \frac{|A_N - A_0|}{A_{max}}, \tag{3}$$

where A_{dif} is the normalised amplitude difference, A_0 is the amplitude of L_{CR} wave before loading, A_N is the amplitude of L_{CR} wave after damage and A_{MAX} is the maximal amplitude under all testing conditions [22].

Taking the pulse-echo mode method, the attenuation coefficient α was calculated according to the following equation:

$$\mathcal{L} = \frac{20}{2d} lg\left(\frac{A_1}{A_2}\right), \tag{4}$$

where d is the specimen thickness, A_1 is the maximum value of amplitude for the first bottom echo and A_2 is the maximum value of amplitude at the second bottom echo [22].

Initially, an amplitude of the L_{CR} wave was captured after different number of loading cycles. It was found that the amplitude values of the L_{CR} wave decrease monotonously with increasing cycles. Subsequently, the following parameters were calculated: A_{dif} of the L_{CR} method, and α of the pulse-echo method. It was found that both A_{dif} and α increased first for the plastic strain to lower than ε_p = 3.2%. If it reached ε_p = 3.2%, the A_{dif} attained the stable stage, whereas the attenuation coefficient α decreased, and subsequently increased slightly just before 1×10^3 fatigue cycles were completed. It has to be mentioned, however, that amplitude difference stabilisation of A_{dif} can be a result of fatigue damage development and surface roughness R_q variation as well. The linear increase in R_q with the number of cycles was observed.

The early stage fatigue damage was considered also in the cast austenite stainless steel CAST by means of both the attenuation coefficient α and electron backscatter diffraction (EBSD) method [23]. The fatigue process was conducted for the frequency f = 2 Hz and cycle asymmetry coefficient R = 0.1. Three magnitudes of stress amplitude were considered: 230 MPa, 250 MPa and 270 MPa [23]. In order to evaluate fatigue damage, the M_L parameter coming from EBSD measurements was taken into account. This parameter was determined based on the analysis of orientation differences between selected points in a grain [24]. As shown in [25], the M_L parameter was important because the grain orientation affects the propagation of ultrasonic waves, and as a consequence, attenuation coefficient α.

With respect to to some limitations of the ultrasonic techniques, particularly in the damage assessments at the early stage of fatigue, another more powerful non-destructive method should be considered that would be able to potentially detect areas where damage appears.

It was decided that the magnetic Barkhausen noise (MBN) method would be suitable to give support in this matter due to its significant sensitivity to material damage, especially in the early stages of degradation. MBN emission is defined as a voltage signal that is generated by non-continuous domain wall movement ina magnetised material due to the discontinuous changes in the magnetic flux density [26]. The domain walls are pinned temporarily by microstructural barriers (voids, dislocations, precipitates, grain boundaries, non-metallic inclusions) to their motion and they are then released abruptly in the changing magnetic field [27]. A type of domain wall depends on the magnetocrystalline anisotropy coefficient [28]. In the case of steel, the domain walls are of 180º and 90º types [29]. There are some publications that describe some attempts for the Barkhausen noise method application in fatigue process monitoring [30–34]. The authors of [30] examined soft steel A48P2, which contains 0.15% C with a ferrite–pearlite microstructure. It is regarded as the most encountered in steam generator pipes. They also tested the alloyed steel 20CDV5 (0.20% C + Cr–Mo–V), which displays a martensitic microstructure. It is frequently used for steam turbine elements such as rotors or bolts. Both materials were subjected to tension/compression cycling under constant strain. In the case of A48P2 steel, the strain amplitudes of ε = ±0.2% and ε = ±0.5% were applied, whereas for the 20CDV5 steel, only one value of strain amplitude was taken into account, ε = ±1%. Guyon and Mayos obtained the following results for the A48P2 steel: in the case of ε = ±0.2% an increase in the maximum amplitude BN_{max} of the Barkhausen noise amplitude was observed, and moreover, a slight decrease in the position of the maximum amplitude HBN_{max}, was easily noticed. For a higher value of strain amplitude (ε = ±0.5%), a decrease in the BN_{max} parameter, and simultaneously, an increase in the HBN_{max} parameter were obtained. Moreover, a second peak appeared for negative values of the applied field [30], and the characteristic change in the shape of the Barkhausen noise envelope occurred continuously throughout the fatigue life of the material [30]. This behaviour can be attributed to

DOI 10.2478/ama-2024-0005

strain hardening due to growing hindrance of the domain wall movement, and as a consequence, an increase in dislocation density [29]. Unlike the soft ferrite–pearlitic A48P2 steel, the martensitic 20CDV5 steel exhibited fatigue softening during cyclic loading: an increase in the BN_{max} parameter with insignificant variations of the HBN_{max} parameter was observed. Moreover, the second peak does not appear [30].

Among the publications describing usage of the Barkhausen noise in evaluation of fatigue damage, the paper by Palit Sagar et al. [33] can be particularly mentioned. The authors examined a low-carbon steel with 0.15%C. The material was subjected to cyclic loading of the stress amplitude equal to 260 MPa and frequency of 10 Hz. It was observed that the maximum amplitude BN_{max} of the Barkhausen emission increased by up to 40% of the material fatigue lifetime and then started to decrease [33].

The measurements carried out by da Silva Junior et al. [32] on SAE8620 steel exhibited a strong sensitivity of the maximum amplitude BN_{max} of Barkhausen noise on the number of cycles in the early stage of damage process development (under a stress level of 259 MPa): a strong increase in the BN_{max} parameter with the number of cycles in the range from 0 to 60 000 cycles was clearly documented [32]. Palma et al. [35] calculated the values of the cumulative Barkhausen noise parameter (BN_{SUM}), according to the equation:

$$BN_{sum} = \sum_{n=0}^{n=n} \left(1 - \frac{v_n}{v_0}\right), \tag{5}$$

where V_n is the root-mean-square (RMS) of Barkhausen voltage for the loaded specimen at the n-th fatigue cycle number, and V_0 is the RMS voltage signal of steel in the as-received state. Similarly as in [32], SAE8620 steel was tested. It was subjected to three levels of stress amplitude: 217 MPa, 259 MPa and 427 MPa. The authors found that BN_{SUM} increases as the number of cycles and stress amplitudes increases [30]. For the stress amplitude close to the fatigue limit of SAE8620 steel (S_e = 194 ±5 MPa), the BN_{SUM} parameter varies only slightly with the fatigue time [35]. Increasing the fatigue stress amplitude leads to an increase of the Barkhausen noise due to major changes in the material microstructure [35].

A shape of the Barkhausen noise envelopes for 14MoV6-3 (1.7715, 13HMF) and X10CrMoVNb9-1 (1.4903, P91) steels was studied in detail by Augustyniak et al. [34], after different levels of fatigue damage.

An innovation of this research is reflected by the fatigue effects analysis carried out simultaneously with the Barkhausen noise method usage. Thanks to such an approach, material damage can be monitored even in the early stages of exploitation, and moreover, the method provided information about the microstructural changes and strain/stress history as well.

2. MATERIAL, SPECIMENS AND EXPERIMENTAL PROCEDURE

The 42CrMo4 steel, also denoted as 1.7225, was selected for the experimental analysis due to its wide applicability, covering different branches of industry, that is motor transport, aviation, power engineering, building construction and so on [36]. One can indicate an application of the 42CrMo4 steel in the energy industry as hollow shafts for wind turbines [37]. Axles, shafts [37], crankshafts [38], connecting rods [39], chain wheels [40], motor cylinders, ball pins and multi-spline shafts [41] can serve as typical examples of structural components where this kind of steel found widespread application. The mentioned application examples show that the material can be effectively used under various types of loading, from static to dynamic.

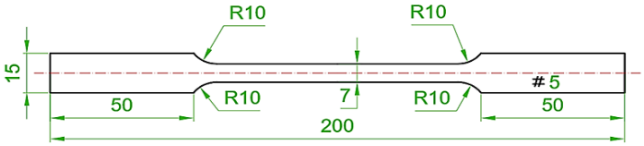

Fig. 1. Engineering drawing of flat specimen for tensile tests

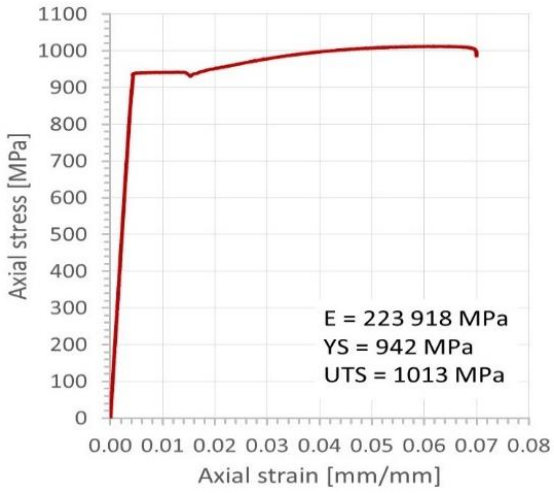

Fig. 2. Tensile characteristic and mechanical parameters of the 42CrMo4 steel in the as-received state: E – Young's modulus, YS – yield stress, UTS – ultimate tensile strength

Three main stages of the experimental procedure, represented by destructive and non-destructive tests and analysis of the relationships between results coming from fatigue and non-destructive magnetic investigation were performed. In the first stage, tensile tests were carried out in order to determine the mechanical parameters of the material in the as-received state. Hence, the flat specimens of geometry and the dimensions shown in Fig. 1 were employed. Standard tensile tests were carried out at room temperature using an 8802 INSTRON servo-hydraulic testing machine and flat specimens. The tests were executed under monotonically increasing loading with a displacement rate of 1 mm/min. Based on the tensile characteristic the following mechanical parameters were determined: Young's modulus (E), yield stress (YS) and ultimate tensile strength (UTS); see Fig. 2. Subsequently, the microstructural observations were performed on polished specimens using light microscopy technique; see Fig. 3. The specimens for microstructural inspections were etched using nital.

Fatigue tests were carried out in the second stage of the experiment. The specimens of the same geometry as for the static tensile tests were manufactured. An axial stress signal in the form of sinusoidal function was applied to control all fatigue tests. Cyclic loading in fatigue tests was characterised by the following parameters: cycle asymmetry coefficient R = 0.1, stress amplitude of 400 MPa and mean stress level of 500 MPa, while the minimum and maximum values of stress ranged from 100 MPa and 900 MPa, respectively; see Fig. 4. The value of maximum stress was

DOI 10.2478/ama-2024-0005

established based on the values of proportional and elastic limits determined from the tensile characteristic.

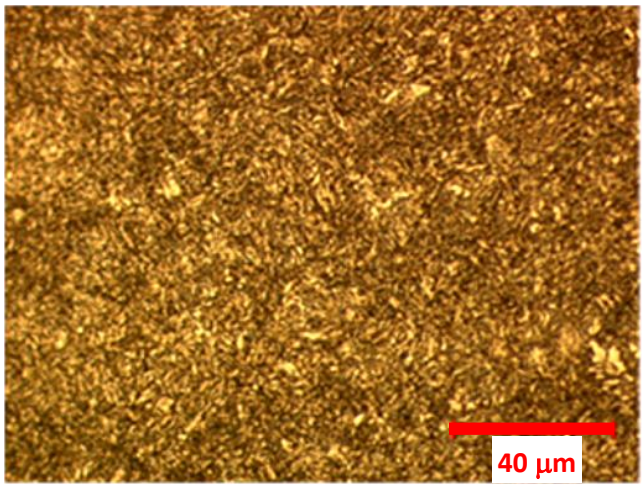

Fig. 3. Microstructure of the 42CrMo4 steel

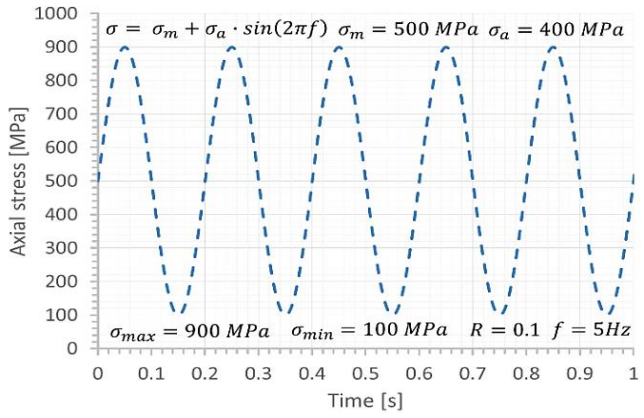

Fig. 4. A scheme of cyclic loading versus time with the main test parameters

The fatigue tests were stopped at defined values of cycle number: 2 510, 7 540, 12 566, 17 590 and 22 620. They correspond to the following lifetime percentage: 10%, 30%, 50%, 70% and 90%, respectively. For each portion of cycles considered, the material was unloaded, and subsequently, subjected to the Barkhausen noise measurements using an MEB-4C defectoscope.

The head of the measuring seat consisted of a U-shaped core of electromagnets wrapped in the wound excitation coil. The pick-up coil was built-in to the sensor. In the pick-up coil, a voltage signal was induced. A triangular waveform was used. The fast-variable component was separated by means of a high-pass filter f = (0-500) Hz. Analysis of this component provided information on the degree of simulated exploitation of the steel tested.

The envelopes of magnetic Barkhausen noise were calculated as rms value U_b according to the equation [29]:

$$U_b = \sqrt{\frac{1}{\tau}\int_0^{\tau} U_{tb1}^2(t)dt}, \tag{6}$$

where U_b [V] is the root mean square of the coil output voltage, U_{tb1} [V] is the fast-variable component defining voltage separated by means of the high-pass filter from the induced voltage in the pick-up coil and τ [s] is the integration time.

Then, the amplitude of Barkhausen noise (Ub_{pp}), defined as the voltage difference between the maximum peak value of the magnetic Barkhausen noise (U_b) and the background noise (U_{tb}), was determined.

In the next step the integral of the half-period voltage signal of MBN was calculated [29]:

$$Int(Ub) = \int_{-Ugmax}^{+Ugmax} U_{sb}\, dU_g, \tag{7}$$

where U_{sb} [V] is the rms of the Barkhausen emission voltage after correction due to background noise, U_b [V] is the rms of the coil output voltage, U_{tb} [V] is the rms of background voltage and U_g [V] is the generator voltage.

Moreover, the full-width at half-maximum (FWHM) of rms envelope of the Barkhausen noise was determined.

In the next stage of the experimental programme, static tensile tests were performed on the specimens after fatigue in order to discover the nature of the material fracture.

3. RESULTS AND DISCUSSION

As it was discovered in this research, the 42CrMo4 steel exhibits very attractive mechanical parameters characterised by high values of yield stress and ultimate tensile strength: 942 MPa and 1013 MPa, respectively; see Fig. 2. This is due to the tempered martensite microstructure of the material in question (Fig. 3) and sufficient carbon content. It has to be emphasised that the proportional limit of this steel equal to 848 MPa is also very beneficial, taking into account a heavy loading of elements that require working conditions without permanent deformation. Thanks to this, 42CrMo4 steel can be treated as the engineering material of mechanical parameters fulfilling the requirements for high-strength steel grades.

Fracture regions of the fatigue pre-strained 42CrMo4 steel subjected to the tensile test, expressed differences in the material degradation, identifying an influence of the fatigue process on the steel response under monotonically increasing tensile force; see Fig. 5. It can be easily noticed that the fracture zones are represented by different sections. In the case of steel tested in the as-received state, two regions can be evidenced. In the middle of the fracture zone, the horizontal plane with longitudinal cracks was dominant, while the border area was represented by the angular plane; see Fig. 5a. This means that decohesion of the steel started under normal stress and was finalised thanks to the combination of shear and normal stress state components. In the case of pre-strained steel, due to fatigue loading history corresponding to 70% of the total fatigue lifetime, that is 17 590, the brittle region became more dominant; see Fig. 5b, and for the cycle numbers 22 620 (90% of the total fatigue lifetime) this region was completely covered by the damage zone; see Fig. 5c.

The shape of the Barkhausen noise envelope changed after the application of fatigue loading; see Fig. 6. RMS Barkhausen noise variations were attributed to the microstructural changes that occurred during the fatigue process. Since tempered martensite contained small cementite particles in the fine-grained ferritic martensite, only a slight increase in the effective voltage value U_b can be observed as the second maximum coming from cementite; see Fig. 6.

The magnetic parameters determined from the rms envelope of the Barkhausen noise were presented as a function of the number of cycles to failure. An increase in the Ub_{pp} parameter in the range from 0% to 10% of the fatigue damage lifetime was

DOI 10.2478/ama-2024-0005

clearly identified. This is because new dislocations appeared in the material due to dynamic loading. According to Moorthy et al. [42], the Barkhausen noise voltage increases when the microstructural features amount *n* and domain walls velocity *v* increase, but simultaneously, the time of flight *t* of domain walls movement between defects decreases. This can be described by the following expression:

$$U_b = \frac{nv}{t}, \tag{8}$$

where: n is the amount of microstructural features, v is the velocity of domain walls and t is the time of flight of domain walls movement between defects.

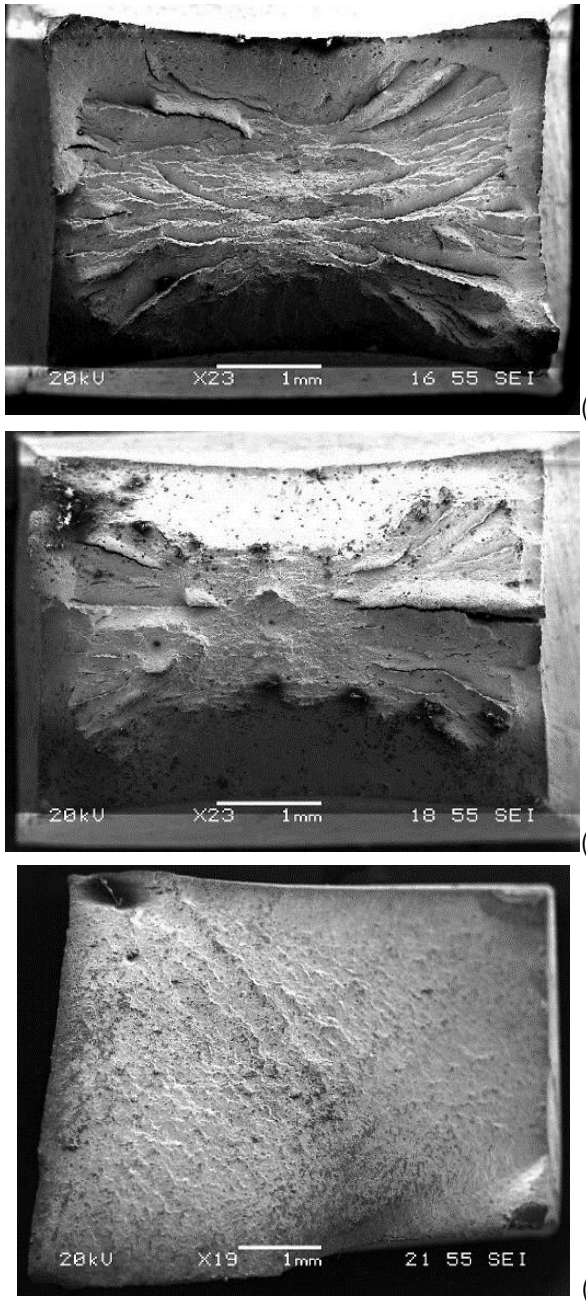

Fig. 5. Fracture zones after tensile tests in the 42CrMo4 steel preloaded due to fatigue for the following parts of the fatigue lifetime: (a) 0%, (b) 70% and (c) 90%

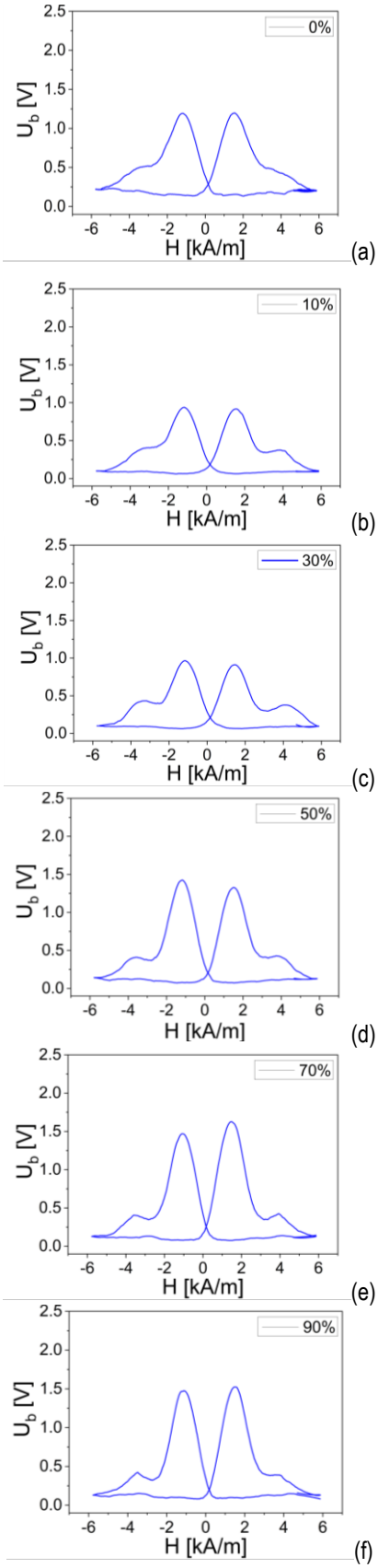

Fig. 6. Envelopes of the rms Barkhausen noise before and after fatigue loading: (a) as-received steel; (b), (c), (d), (e) and (f) steel tested under fatigue interrupted after 10%, 30%, 50%, 70% and 90% of the total lifetime of the material, respectively

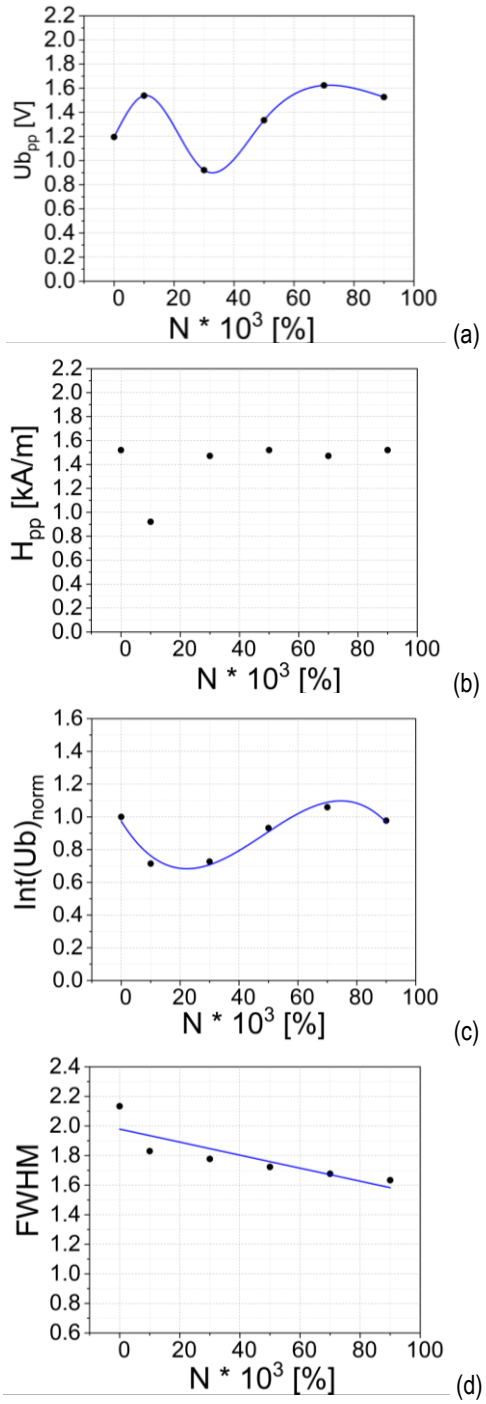

Fig. 7. Magnetic parameters determined from the rms Barkhausen noise envelope versus percentage of fatigue lifetime

As stated by Sagar et al. [33], the initial increase in Barkhausen noise amplitude can be attributed to the dislocation rearrangements and formation of cell structures. However, one can notice that these tests were carried out by this research team on low-carbon steel of the carbon content higher by weight of about 2.7 times in comparison to the steel tested in this research.

The results obtained for the fatigue pre-strained steel of up to 30% of the total fatigue lifetime show that the value of the Ubpp parameter decreases. This effect can be attributed to the increase in dislocation density, which hinders the movement of the domain walls in the material [33]. As a consequence, a less number of the domain walls were able to move due to stronger pinning [33]. Sagar et al. [33] also observed a reduction in the dislocation cell size in the low-carbon steel tested.

Another possible reason for the Barkhausen noise amplitude decrease is the persistent slip bands (PSBs) formation in the material due to dynamic loading [33]. The accumulation of deposited dislocations on the PSB–material matrix interfaces causes during fatigue three-dimensional residual compression stress in PSBs [43]. However, it is well known [27, 44, 45] that compressive stresses reduce the Barkhausen noise level in materials with a positive coefficient of magnetocrystalline anisotropy K. Steels belong to such materials.

Taking into account the results of the steel fatigue pre-strained for the higher number of loading cycles (exceeding 30% of the number of cycles to failure), the Barkhausen noise level, expressed as the Ub_{pp} parameter, increases. Under such testing conditions, the crack initiates, and then, the stress relaxation takes place, leading as a consequence to Ub_{pp} increase [33]. The trends in increase or decrease of the Ub_{pp} parameter of the medium carbon steel are very similar to those presented in the literature [32] for the SAE8620 steel.

Earlier publications did not pay attention to the magnetic parameters determined from the Barkhausen noise rms envelope, such as Int(Ub), H_{pp} and FWHM [32, 33, 46]. It turns out that changes in these parameters considered as a function of the number of loading cycles have a completely different character. For example, a linear decrease in the FWHM parameter versus the cycles to failure was observed.

4. CONCLUSIONS

Magnetic Barkhausen effect was used to identify the damage degree of the 42CrMo4 medium carbon steel subjected to fatigue loading conditions. The rms Barkhausen noise envelope follows material degradation due to cyclic loading, and as a consequence evolution of dislocation structure.

Among the considered parameters, FWHM is the most suitable since it changes linearly with the increasing number of loading cycles, thus giving fast assessments of the material degradation. It decreases with the duration of the fatigue process and damage development.

The linear character of the relationship between the FWHM parameter and the number of loading cycles to fracture was discovered, providing the promising tool for early fatigue damage inspection. This means the method can support diagnostic and inspection processes of elements and structural metallic materials with the application of other non-destructive methods.

REFERENCES

1. Heyes AM. Automotive component failures. Eng Fail Anal. 1998;5(2):129–141. Available from: https://doi.org/10.1016/S1350-6307(98)00010-7
2. Meyers MA., Chawla KK. Mechanical behaviour of materials. Cambridge University Press, Cambridge, second edition, 2009.
3. Bhaumik SK. Fatigue fracture of crankshaft of an aircraft engine. Eng Fail Anal. 2002;9(3):255–263. Available from: https://doi.org/10.1016/S1350-6307(01)00022-X
4. Fonte M, Anes V, Duarte P, Reis L, Freitas M. Crankshaft failure analysis of a boxer diesel motor. Eng Fail Anal. 2015;5:109–115. Available from: https://doi.org/10.1016/j.engfailanal.2015.03.014
5. Godec M, Mandrino Dj, Jenko M. Investigation of the fracture of car's drive shaft. Eng Fail Anal. 2009;16(4):1252–1261. Available from: https://doi.org/10.1016/j.engfailanal.2008.08.022

6. Tjernberg A. Fatigue lives for induction hardened shafts with subsurface crack initiation. Eng Fail Anal. 2002; 9(1):45–61. Available from: https://doi.org/10.1016/S1350-6307(00)00036-4
7. Yu Z, Xu X. Failure analysis of an idler gear of diesel engine gearbox. Eng Fail Anal. 2006;13:1092–1100. Available from: https://doi.org/10.1016/j.engfailanal.2005.07.015
8. Chen B, Wang C, Wang P, Zheng S, Sun W. Research on fatigue damage in high-strength steel (FV520B) using nonlinear ultrasonic testing. Shock and Vibration 2020; 8(19):1–15. Available from: https://doi.org/10.1155/2020/8847704
9. Sarris G, Haslinger SG, Huthwaite P, Lowe MJS: Ultrasonic methods for the detection of near surface fatigue damage. NDT & E Int. 2023;135:1–13. Available from: https://doi.org/10.1016/j.ndteint.2023.102790
10. Kowalczyk D, Aniszewicz A. Experimental and simulation tests of 1MN screw coupling. Problemy Kolejnictwa. Rail. Rep. 2022;194: 97–102. Available from: https://doi.org/10.36137/1943E
11. Bjørheim F, Siriwardane SC, Pavlou D. A review of fatigue damage detection and measurement techniques. Int. J. Fat. 2022;154:1–16. Available from: https://doi.org/10.1016/j.ijfatigue.2021.106556
12. Wu H, Ziman JA, Raghuraman SR, Nebel J-E, Weber F. Starke P.: Short-time fatigue life estimation for heat treated low carbon steels by applying electrical resistance and magnetic Barkhausen noise. Materials. 2023;16:1–21.
Available from: https://doi.org/10.3390/ma16010032
13. Roye W. Ultrasonic testing of spot welds in the automotive industry. Krautkramer, SD 298, 11/99, 6 pages.
14. Yuhas DE, Vorres CL, Remiasz JR, Gesch E, Yamane T. Nondestructive ultrasonic methods for quality assurance of brake pads. EuroBrake. 2012, April 16- 18th 2012, Dresden Germany.
15. Lamarre A. Ultrasonic phased-array for aircraft maintencance, Amstredam, November 2009, 76 slides. Available from: https://ndt.aero/images/docs/UTPAfor%20maintenance.pdf
16. Wronkowicz A, Dragan K. Damage evaluation based on ultrasonic testing of composite aircraft elements and image analysis methods. MATEC Web of Conferences 204, IMIEC 2018, 06003. Available from: https://doi.org/10.1051/matecconf/201820406003
17. Luziński R, Ziemkiewicz J, Synaszko P, Zyluk A, Dragan KA. Comparison of composite specimens damage area measurements performed using pulsed thermography and ultrasonic NDT methods. Fat. Air. Struc. 2019; 2019(11): 68–77.
Available from: https://doi.org/10.2478/fas-2019-0007
18. Drelich R, Rosiak M, Pakuła M. Application of non-contact ultrasonic method in air to study fiber-cement corrugated boards, Bull. Pol. Ac. Tech., 2021;69(2).
Available from: https://doi.org/10.24425/bpasts.2021.136740
19. Callejas A, Palma R, Hernández-Figueirido D, Rus G. Damage detection using ultrasonic techniques in Concrete-Filled Steel Tubes (CFSTS) columns. Sensors. 2022;22,4400. Available from: https://doi.org/10.3390/s2212440
20. Mackiewicz S. Possibilities of ultrasonic evaluation of energetic steels as a result longterm exploitation (in Polish). Materiały Konferencyjne VII Sympozjum Informacyjno-Szkoleniowe „Diagnostyka i remonty długoeksploatowanych urządzeń energetycznych. Nowe problemy diagnostyczne na starych blokach energetycznych", 05–07 October 2005, Ustroń, Poland.
21. Hirao M, Ogi H, Suzuki N, Ohtani T. Ultrasonic attenuation peak during fatigue of polycrystalline copper. Acta Mater. 2000;48:517–524. Available from: https://doi.org/10.1016/S1359-6454(99)00346-8
22. Luo Z, Meng Y, Fan S, Lin L. Assessment of surface/subsurface damage in early-stage fatigue: A new attempt based on LCR wave. Int. J Fat. 2023;170:107537. Available from: https://doi.org/10.1016/j.ijfatigue.2023.107537
23. Luo Z, Wang X, Ma Z, Zou L, Zhu X, Lin L. Combined quantitative evaluation on early-stage fatigue damage of coarse-grained austenite stainless steel based on EBSD and ultrasonic technique. Ultrasonics 2020;103:106090. Available from: https://doi.org/10.1016/j.ultras.2020.106090
24. Kamaya M, Kuroda M. Fatigue damage evaluation using backscatter diffraction. Mater. Trans. 2011;52:1168–1176.
Available from: https://doi.org/10.1016/S1359-6454(99)00346-810.2320/matertrans.M2011014
25. Luo Z, Dong H, Ma Z, Zou L, Zhu X, Lin L. Orientation relationship between ferrite and austenite and its influence on ultrasonic attenuation in cast austenitic stainless steel. Acta Physica Sinica. 2018;67: 238102. Available from: https://doi.org/10.7498/aps.67.20181251.
26. Piotrowski L, Augustyniak B, Chmielewski M, Tomaš I. The influence of plastic deformation on magnetoelastic properties of the CSN12021 grade steel. J Magn Magn Mater. 2009;321(15):2331–2335. Available from: https://doi.org/10.1016/j.jmmm.2009.02.028
27. Blaow M, Evans JT, Shaw BA. The effect of microstructure and applied stress on magnetic Barkhausen emission in induction hardened steel. J Mater Sci. 2007;42(12):4364–4371. Available from: https://doi.org/10.1007/s10853-006-0631-5
28. Piech T. Magnetic research. Application of Barkhausen effect (in Polish). Biuro Gamma, Warsaw, 1998.
29. Jiles D. Introduction to magnetism and magnetic materials. CRC Press, Boca Raton. 1998.
30. Guyon M, Mayos M. Nondestructive evaluation of fatigue damage of steels using magnetic techniques. Review of Progress in Quantitative Nondestructive Evaluation. 14. Edited by D.O. Thompson and D.E. Chimenti, Plenum Press, New York, 1995, 1717–1724.
31. Palma ES, Mansur TR, Ferreira Silna Jr S, Alvarenga Jr A. Fatigue damage assessment in AISI 8620 steel using Barkhausen noise. Int J Fat. 2005;27(6):659-665.
Available from: https://doi.org/10.1016/j.ijfatigue.2004.11.005
32. da Silva Junior SF, Mansur TR, Aguiar AE, Palma ES, Marques PV. Damage accumulation study in fatigue testing using Barkhausen noise. Proceedings of COBEM 2003, 17th International Congress of Mechanical Engineering, 10–14 November 2003, Sao Paulo, Brazil. Available from: https://www.abcm.org.br/anais/cobem/2003/html/pdf/COB03-0558.pdf
33. Sagar PS, Parida N, Das S, Dobmann G, Bhattacharya DK. Magnetic Barkhausen emission to evaluate fatigue damage in a low carbon structural steel. International Journal of Fatigue. 2005;27(3): 317–322.
Available from: https://doi.org/10.1016/j.ijfatigue.2004.06.015
34. Augustyniak B, Piotrowski L, Chmielewski M, Kowalewski Z. Comparative study with magnetic techniques of P91 and 13HMF steels properties subjected to fatigue tests. J Elec Eng. 2012;63(7):15–18.
Available from: http://iris.elf.stuba.sk/JEEEC/data/pdf/7s_112-04.pdf.
35. Palma ES, Junior AA, Mansur TR, Pinto JMA. Fatigue damage in AISI/SAE 8620 steel. Proceedings of COBEM 2003, 17th International Congress of Mechanical Engineering, 10–14 November 2003, Sao Paulo, Brazil. Available from: https://www.abcm.org.br/anais/cobem/2003/html/pdf/COB03-0066.pdf
36. Morsy MA, El-Kashif E. Repair welding reclamation of 42CrMo4 and C45 steels. Proceedings of IIW 2017 International Conference, June, 29-30 Shanghai, R.P. China.
37. Costa LL, Brito AMG., Rosiak A, Schaeffer L. Microstructure evolution of 42CrMo4 during hot forging process of hollow shafts for wind turbines. Int. J Adv. Man. Tech. 2020; 106:511–517.
Available from: https://doi.org/10.1007/s00170-019-04642-w
38. Fischer A, Scholtes B, Niendorf T. Influence of deep rolling and induction hardening on microstructure evolution of crankshaft sections made from 38MnSiVS5 and 42CrMo4. HTM-J Heat Treat Mater. 2021;76:175-179. Available from: https://doi.org/10.1515/htm-2021-0002
39. Basavaraj Y, Joshi R, Setty GR. FEA of NX-11 unigraphics modelled connecting rod using different materials. Mater Today: Proc. 2021;46:2807–2813.
Available from: https://doi.org/10.1016/j.matpr.2021.02.620
40. Wieczorek AN. Studies on the combined impact of external dynamic forces and quartz abrasive on the wear of chain wheels made of 42CrMo4 steel which are used in conveyors [in Polish]. Autobusy. 2016;6:1207–1210.

41. Das S, Mukhopadhyay G, Bhattacharyya S. Failure analysis of axle shaft of a fork lift. Case Studies in Eng Fail Anal. 2015;3:46–51. Available from: https://doi.org/10.1016/j.csefa.2015.01.003
42. Moorthy V, Choudhury BK, Vaidyanathan S, Jayakumar T, Rao KBS, Raj B. An assessment of low cycle fatigue using magnetic Barkhausen emission in 9Cr-1Mo ferritic steel. Int J Fat. 1999;21(3):263–269. Available from: https://doi.org/10.1016/S0142-1123(98)00079-6
43. Polák J, Man J. Mechanisms of extrusion and intrusion formation in fatigue crystalline materials. Mater Sci Eng A. 2014;596:15-24. Available from: https://doi.org/10.1016/j.msea.2013.12.005
44. Anglada-Rivera J, Padovese LR, Capó-Sánchez J. Magnetic Barkhausen noise and hysteresis loop in commercial carbon steel: influence of applied tensile stress and grain size. J Magn Magn Mater. 2001;231(2-3):299–306. Available from: https://doi.org/10.1016/S0304-8853(01)00066-X
45. Stewart DM, Stevens KJ, Kaiser AB. Magnetic Barkhausen noise analysis of stress in steel. Curr Appl Phys. 2004;4(2-4):308–311. Available from: https://doi.org/10.1016/j.cap.2003.11.035
46. Tomita Y, Hashimoto K, Osawa N. Nondestructive estimation of fatigue damage for steel by Barkhausen noise analysis. NDT & E Inter. 1996;29(5):275–280. Available from: https://doi.org/10.1016/S0963-8695(96)00030-8

Katarzyna Makowska: https://orcid.org/0000-0002-7348-8700

Tadeusz Szymczak: https://orcid.org/0000-0003-2533-7200

Zbigniew L. Kowalewski: https://orcid.org/0000-0002-8128-0846